Submillimeter-resolution magnetic resonance imaging at the Earth's magnetic field with an atomic magnetometer

Shoujun Xu,[1] C. W. Crawford,[1] Simon Rochester,[2] Valeriy Yashchuk,[3] Dmitry Budker,[2,*] and Alexander Pines[1,†]
[1]*Department of Chemistry, University of California, Berkeley, California 94720, USA*
and Materials Sciences Division, Lawrence Berkeley National Laboratory, Berkeley, California 94720, USA
[2]*Department of Physics, University of California, Berkeley, California 94720, USA*
and Nuclear Sciences Division, Lawrence Berkeley National Laboratory, Berkeley, California 94720, USA
[3]*Advanced Light Source, Lawrence Berkeley National Laboratory, Berkeley, California 94720, USA*
(Received 25 October 2007; published 7 July 2008)

Magnetic resonance imaging in the Earth's magnetic field is achieved using a sensitive atomic magnetometer for detection. We demonstrate images with a submillimeter resolution by recording the flow of two water paths meeting at a *T*-shaped mixer. The high homogeneity of the Earth's field allows the use of weak gradient fields which circumvent the concomitant-field effect. To distinguish the two input channels, we employed selective polarization, which is a unique and noninvasive labeling method for low-field magnetic resonance imaging. Our technique imposes minimal physical constraints on the object under study, in contrast to conventional high-field magnetic resonance imaging. This technique is applicable for microfluidic imaging in laboratory-on-a-chip devices.

DOI: 10.1103/PhysRevA.78.013404 PACS number(s): 33.25.+k, 42.79.Pw

Controlling chemical and biological processes, such as separations and reactions carried out on laboratory-on-a-chip devices, requires detailed information regarding flow dynamics, mixing behavior, and analyte distribution in the numerous channels on the chip [1–3]. The most common techniques for monitoring the flow phenomena in microchannels involve fluorescence detection [4–6]. While they offer high sensitivity, the required labeling with fluorescent reagents is undesirable in many applications. Other techniques, such as chromatography and mass spectrometry, are normally inapplicable to noninvasive, in-line analysis of multiple-step processes [7]. Conventional nuclear magnetic resonance (NMR) and magnetic resonance imaging (MRI) are noninvasive and capable of chemical identification, but the magnetic-susceptibility differences between the analyte and the chip materials have to be compensated for [8]. Recently Harel *et al.* reported a high-field MRI study of flow in a microfluidic chip using remote detection, in which the encoding and detection are separated; the susceptibility issue was circumvented and the detection sensitivity was greatly improved [9]. However, measurements performed using bulky superconducting magnets are often impossible or inconvenient for practical applications, especially those required to be conducted outside of laboratories. One possible solution is to conduct magnetic resonance measurements in a low magnetic field, for example, the Earth's magnetic field. Mohorič *et al.* and Halse *et al.* have explored the potential of MRI in the Earth's magnetic field with conventional induction detection [10,11]. Unfortunately, the intrinsically low sensitivity of Faraday detection in such a low field demands a substantial amount of sample, making it impractical for microfluidic studies. Therefore alternative detection techniques for magnetic resonance in low-field are desirable.

One approach is to use a superconducting quantum interference device (SQUID) as the detector [12]. Significant progress has been made by Clarke and co-workers [13,14]. Here we demonstrate a laser-detected MRI technique that can be applied to microfluidic imaging and, unlike SQUID MRI, does not require cryogenics. The methodology employs ultrasensitive laser-based atomic magnetometers as detectors [15]. The sensitivity is independent of the strength of the magnetic field and the experiments can therefore be carried out in an arbitrarily low field without suffering signal loss.

The principle of laser detection of magnetic resonance has been described previously [16–18]. Briefly, our atomic magnetometers are based on nonlinear magneto-optical rotation of the light polarization by an alkali metal vapor. In the presence of an external magnetic field, which is the vector sum of a constant bias field and the magnetic field of the sample, the ground state of the alkali metal atoms undergoes Zeeman splitting. A polarized laser beam with appropriate wavelength selectively excites a certain combination of the Zeeman sublevels, generating an alignment of the angular momentum in the ground state of the alkali metal atoms. The resulting atomic polarization precesses in the external magnetic field and consequently rotates the polarization of the incident laser beam. If the laser light is modulated in frequency or amplitude, a resonance in optical rotation occurs when the modulation of the laser is synchronized with the precession. The magnitude of the magnetic field can therefore be deduced from the corresponding modulation frequency of the laser when resonance is observed.

We report an imaging study of mixing of two otherwise identical fluids with nuclear-spin labeling. The spatial resolution reaches the submillimeter regime, nearly five times better than conventional MRI detection in the same leading field [11]. The detection limit and spatial resolution will be greatly improved when the detector is optimally implemented with microfluidic chips. The apparatus incorporates

*Corresponding author. budker@berkeley.edu
†pines@berkeley.edu

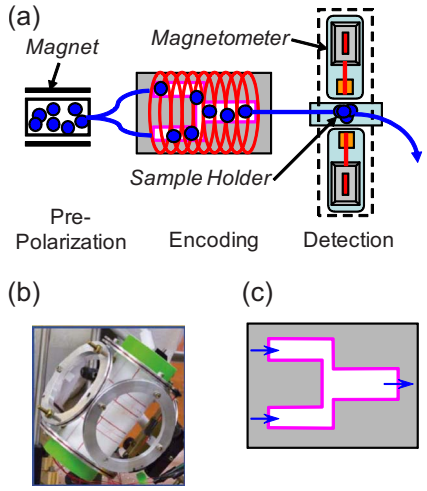

FIG. 1. (Color online) (a) Schematic of the experimental setup. Three regions are shown: prepolarization, encoding, and detection. Blue dots represent the analyte. Blue lines indicate the tubes in which water flows from one region to another. (b) Earth's field MRI encoding system, approximately cubic in shape, 15-cm side length. The compensating coils are mounted on three pairs of aluminum rings. The gradient coils are wound around a Teflon tube. A second Teflon tube with a smaller diameter, on which a saddle coil for excitation is mounted, is inserted into the gradient-coil holder. The bore size for this imaging system is 2.5 cm diameter. (c) Imaging phantom. *T*-shaped mixer, consisting of two input channels and one output channel.

only low power, highly integrable electronics, allowing miniaturization and development of a portable battery-operated device. With these modifications, we expect laser-detected MRI to be a unique and versatile analytical tool for the expanding field of microfluidics.

The schematic of our setup is shown in Fig. 1(a). It consists of prepolarization, encoding, and detection regions. Water, driven by 6.5 atm nitrogen gas with a flow rate of 30 ml/min, passes (when desired) through a 0.3-T magnetic field for prepolarization. Then it flows into the encoding region where the spatial information of the nuclear spins in the imaging phantom is stored. The residence time of water in the encoding region is about 800 ms. The encoded water is then introduced into a sample holder which is located inside a piercing solenoid and in the vicinity of the atomic magnetometers to read out the images. The solenoid piercing through the magnetic shield provides a leading field, which is not experienced by the magnetometers, for the nuclear spins.

Figure 1(b) shows the spatial encoding system in the Earth's (or, more precisely, unshielded laboratory) field. It contains three pairs of anti-Helmholtz coils to cancel possible magnetic gradients in the laboratory (not in use for the experiments presented here), a saddle coil for excitation (not tuned to the resonance frequency due to the low Larmor frequency at the Earth's field), and three-axis gradient coils for spatial encoding. The gradient coils are of standard geometry: one Maxwell coil for the direction along the leading field (z axis), and two double Golay coils for the transverse directions (x and y axes). The compensating coils are mounted on aluminum rings. The excitation coil and gradient coils are wound on a Teflon holder. The nominal value of the field in the laboratory is 42 μT, corresponding to a Larmor frequency of 1.78 kHz (an audio frequency) for protons.

The imaging phantom is comprised of two smaller channels on the input side, and one larger channel on the output side for mixing [Fig. 1(c)]. All the channels are 12 mm long. The diameters are 3.2 mm for the input channels and 4.5 mm for the output channel, so that the volume of the output channel is the sum of the volumes of the input channels.

For spatial encoding, a two-dimensional phase encoding pulse sequence is used [15]: the duration of the excitation pulse is 5 ms; the step sizes of the gradient fields are 0.2 and 0.1 μT/mm for the z and y axes, respectively; the duration for the gradient-field pulses is 10 ms. The amplitude of the gradients is carefully chosen so that (a) it is significantly greater than the inhomogeneity of the Earth's field in the laboratory, which is 0.02 μT/mm, and (b) the field change on the sample region due to the applied gradients is much smaller than the leading field, to avoid concomitant-field effect. The images are obtained by Fourier transform of the measured magnetization values under various gradient strengths.

The detection apparatus used in this work has been described elsewhere [19]. It is a gradiometer formed by two identical atomic magnetometers arranged so as to cancel out common-mode noise. The magnetometers are enclosed in a magnetic shield. Encoded sample flows into the detection region, which has a volume of 0.4 ml. The nuclear spins are guided by an ~40 μT field generated with a solenoid surrounding the flow channel and piercing the magnetic shield. The magnetic fields from the sample that the two sensors experience are of opposite sign. Thus the difference signal between the two magnetometers represents twice the magnetization of the sample, while common-mode noise is eliminated. The sensitivity for the differential channel of the current apparatus is about 80 fT/Hz$^{1/2}$ for the near-dc signal.

We first study the flow in the whole phantom with both input channels occupied by polarized water. Displayed in Fig. 2, the images show a symmetric flow in the phantom from the two input channels since they are of identical sizes. The output channel has a stronger signal because the diameter of the channel is bigger than the input channels and consequently contains more water sample. For the overall flow, the onset of the significant signal is apparent after 0.4 s, arising from the water at the end of the output channel as it has the shortest travel time to the detectors. At 0.8 s, all the encoded water in the mixing channel arrives at the detection volume, as indicated by the intensity distribution in the corresponding image. The signal subsequently decreases gradually until it disappears after about 2.2 s.

In order to study mixing, we need to be able to distinguish between the water samples from the two input channels. To achieve this, we introduce polarized water through one of the two input channels (the left channel in this study), and unpolarized water through the other channel (Fig. 3). This spin labeling of the sample via selective polarization is useful in low-field MRI for which the encoding field is sufficiently low that it produces no significant polarization on the samples, while in high-field experiments the entire sample will be polarized in the encoding region.

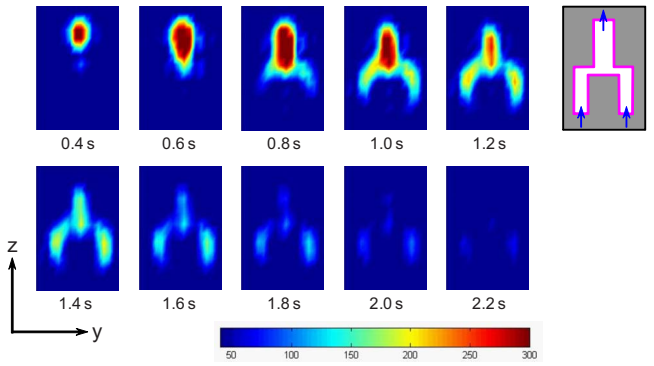

FIG. 2. (Color online) Time-resolved flow images. The color scale indicates relative intensity. The time indicated underneath each image shows the travel time required for the encoded water sample to reach the detectors after an encoding sequence. The connection volume between the encoding and detection stages is negligible compared to the encoding volume and detection volumes. The images are obtained from signals averaged over 30 measurements.

The images show no observable signal from the unpolarized water in the right channel. Only the left channel, containing water polarized in the 0.3-T field, is present in MR images. The resolution is 3 mm for the z axis and 2.5 mm for the y axis. The total signal is approximately half of the signal observed when both channels are filled with polarized water.

Selective polarization of a specific channel is of great value for studying flow and mixing in microchips. It is a noninvasive labeling method involving only nuclear spins. The flow dynamics and distribution of the reactant loaded through the labeled channel can be obtained before, during, and after it undergoes chemical reactions. Unlike other chemical labeling methods, such as commonly used fluorescent labeling and magnetic labeling, the nuclear-spin labeling does not perturb the ongoing reactions or biological processes. Our technique is also superior to selective pulses employed in high-field MRI because it is applicable to a channel with arbitrary shape and multiple channels, whereas

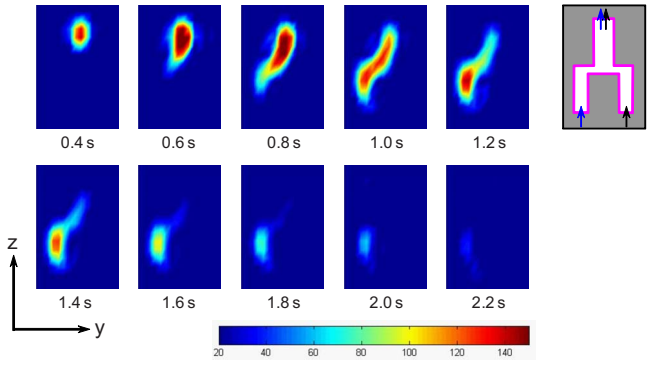

FIG. 3. (Color online) Time-resolved flow images of selectively polarized water. In this case, only water in the left input channel is polarized by the 0.3-T magnetic field. Note the scale of color mapping for imaging intensity is one-half of the scale used in Fig. 2. Other conditions remain the same as those for previous imaging experiments.

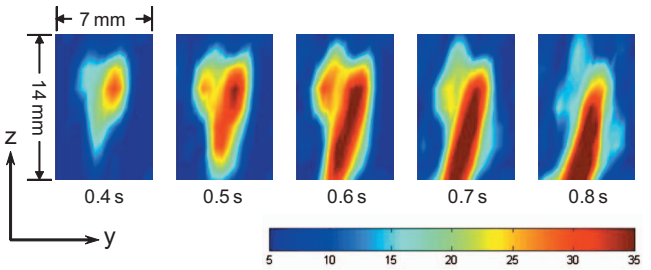

FIG. 4. (Color) High-resolution images of mixing in the output channel. Gradient field is 0.2 μT/mm for the z axis and 0.4 μT/mm for the y axis. All other parameters remain the same as the ones for Fig. 3.

high-field MRI is limited only to one slice or one voxel in the encoding volume.

In order to reveal details of the mixing process, we decrease the imaging field-of-view by increasing the step size of the gradient along the y axis, to focus on the output channel alone where mixing takes place (Fig. 4). The resolution is 0.7 mm along y, the mixing axis, and 3 mm along the flow axis. The images here are obtained from the Fourier transform of signals averaged from 50 measurements. The spatial resolution is substantially better than that of induction detection performed in the same Earth's field [11].

The images shown in Fig. 4 reveal interesting flow behavior. The polarized stream flows across the center line and then spreads out ~6 mm downstream of the joint. If a chemical reaction is designed to occur in this structure, under our experimental conditions it will only take place after the spreading so that different reactants from separate channels will come into contact. In order to gain reasonable yield, the mixing channel is thus required to be longer than 6 mm with the current chip under the same flow conditions. Such information is vital to the design of microchannels in which chemical reactions and biological processes take place.

Earth's field MRI is advantageous compared to high-field MRI in terms of portability, sample size, magnetic susceptibility effects, and power consumption. The entire encoding setup is portable; the encoding volume can be as big as any object to be imaged, which is not possible with superconducting magnets; no accessories are needed to generate the leading field since the Earth's field is always available; the maximum current for gradient fields used in this work is 2 A, compared to many tens of amperes typically used in high-field measurements to generate ~100 μT/mm gradients; and the audio frequency for excitation only needs to be of modest amplitude. Thus our methodology is convenient for applications in microchips.

Compared to our previous work [15], which was conducted in a 3.4 mT magnetic field generated by a solenoid, the current work takes advantage of the ubiquitous and homogeneous Earth's magnetic field. No electronics is necessary. Concomitant-field effect is avoided when we image microchannels due to the small field-of-view and high homogeneity of the Earth's field.

Several possibilities for improving the spatial resolution can be considered. One is to increase the polarization of the

nuclei in the fluid. In addition to using a stronger magnetic field for prepolarization, techniques including hyperpolarization of noble gases [20], parahydrogen [21], and dynamic nuclear polarization [22] can be adopted. Another approach is to improve the detection sensitivity. The theoretical limit of laser detection is on the order of 0.1 $\mathrm{fT}/\mathrm{Hz}^{1/2}$ for a 1 cm^3 detection cell filled with potassium [23]. Various strategies can be adopted to approach this limit, including minimizing optical noise and optimizing the atomic composition in the detecting cells. A third method is to bring the detectors closer to the sample with miniaturized sensor cells [24]. The coupling of the sample and the detectors will thus be significantly improved. We expect that a spatial resolution on the order of tens of micrometers should be achievable. With the wealth of information obtainable using our technique, we hope that it can contribute to the characterization of chemical and biomedical processes on laboratory-on-a-chip devices.

This work was supported by the Director, Office of Science, Office of Basic Sciences, Materials Sciences Division of the U.S. Department of Energy under Contract No. DE-AC03-76SF00098. D.B. acknowledges support by an ONR MURI grant and the Nuclear Sciences Division of the U.S. Department of Energy.

[1] D. Janasek, J. Franzke, and A. Manz, Nature (London) **442**, 374 (2006).
[2] H. Song, H.-W. Li, M. S. Munson, T. G. Van Ha, and R. F. Ismagilov, Anal. Chem. **78**, 4839 (2006).
[3] D. Sinton, Microfluid. Nanofluid. **1**, 2 (2004).
[4] C. Yi, Q. Zhang, C.-W. Li, J. Yang, J. Zhao, and M. Yang, Anal. Bioanal. Chem. **384**, 1259 (2006).
[5] P. S. Dittrich and A. Manz, Anal. Bioanal. Chem. **382**, 1771 (2005).
[6] K. B. Mogensen, H. Klank, and J. P. Kutter, Electrophoresis **25**, 3498 (2004).
[7] N. Lion *et al.*, Electrophoresis **24**, 3533 (2003).
[8] D. L. Olson, M. E. Lacey, and J. V. Sweedler, Anal. Chem. **70**, 645 (1998).
[9] E. Harel, C. Hilty, K. Koen, E. E. McDonnell, and A. Pines, Phys. Rev. Lett. **98**, 017601 (2007).
[10] A. Mohorič, G. Planinšič, M. Kos, A. Duh, and J. Stepišnik, Instrum. Sci. Technol. **32**, 655 (2004).
[11] M. E. Halse *et al.*, J. Magn. Reson. **182**, 75 (2006).
[12] R. Kleiner, D. Koelle, F. Ludwig, and J. Clarke, Proc. IEEE **92**, 1534 (2004).
[13] S. K. Lee *et al.*, Magn. Reson. Med. **53**, 9 (2005).
[14] M. Mößle *et al.*, IEEE Trans. Appl. Supercond. **15**, 757 (2005).
[15] S.-J. Xu *et al.*, Proc. Natl. Acad. Sci. U.S.A. **103**, 12668 (2006).
[16] D. Budker *et al.*, Rev. Mod. Phys. **74**, 1153 (2002).
[17] I. K. Kominis, T. W. Kornack, J. C. Allred, and M. V. Romalis, Nature (London) **422**, 596 (2003).
[18] V. V. Yashchuk, J. Granwehr, D. F. Kimball, S. M. Rochester, A. H. Trabesinger, J. T. Urban, D. Budker, and A. Pines, Phys. Rev. Lett. **93**, 160801 (2004).
[19] S.-J. Xu *et al.*, Rev. Sci. Instrum. **77**, 083106 (2006).
[20] B. M. Goodson, J. Magn. Reson. **155**, 157 (2002).
[21] C. R. Bowers and D. P. Weitekamp, J. Am. Chem. Soc. **109**, 5541 (1987).
[22] C.-G. Joo, K.-N. Hu, J. A. Bryant, and R. G. Griffin, J. Am. Chem. Soc. **128**, 9428 (2006).
[23] D. Budker and M. V. Romalis, Nat. Phys. **3**, 227 (2007).
[24] S. Knappe *et al.*, J. Opt. A, Pure Appl. Opt. **8**, S318 (2006).